The importance of accurately representing submerged vegetation morphology in the numerical prediction of complex river flow

Authors and Affiliations:

Richard J. Boothroyd[1], Richard J. Hardy[1], Jeff Warburton[1] and Timothy I. Marjoribanks[1]

[1] Department of Geography, Durham University, Durham, DH1 3LE, UK.

E-mail: r.j.boothroyd@durham.ac.uk

Abstract:

This paper reports a novel method for the incorporation of complex plant morphologies into a computational fluid dynamics (CFD) model, allowing the numerical prediction of flows around individual plants. The morphological complexity, which comprises the vertical and lateral distribution of individual branches and leaves is captured through terrestrial laser scanning (TLS) and is maintained in the numerical prediction of flow fields. This is achieved where the post-processed, voxelised plant representation is incorporated into a CFD scheme through a mass flux scaling algorithm (MFSA). Flow around *Prunus laurocerasus* has been modelled under foliated and defoliated states following the removal of leaves. The complex plant morphologies are shown to produce spatially heterogeneous downstream velocity fields, with velocity profiles that deviate significantly from the idealised inflected shape. Rapid transition between the high velocity free stream zone and the zone of reduced velocity in the plant wake indicate shearing of flow, with the point of reattachment extending up to seven plant lengths

downstream. The presence of leaves significantly modifies the flow field response, with development of a second, more pronounced wake structure around the dense foliage. This approach provides a full flow numerical description of the pressure field, enabling the vegetative drag force to be quantified. For the example given here, drag force is an order of magnitude greater for the foliated state. The methodology outlined here demonstrates the importance of accurately representing complex plant morphology in hydraulic models, and allows drag forces and coefficients to be calculated for specific plant species.

Keywords:

CFD, Channel vegetation, Terrestrial Laser Scanning, Drag coefficient

Introduction:

Vegetation is abundant in lowland rivers and has a profound influence on the fluvial system. It affects the mean and turbulent flow field (Nepf, 2012a), provides habitat, alters light availability and temperature, and regulates concentrations of oxygen, carbon, and nutrients (Carpenter and Lodge, 1986). A correct understanding of the influence of vegetation on flow is therefore essential and in particular its contribution as an additional form of flow resistance (Kadlec, 1990). Increased flow resistance produces higher water levels per unit discharge, thus increasing the risk of flooding. However, a numerical description of the flow around river channel vegetation canopies is challenging given the multitude of scales to be considered (Nepf, 2012b) and the species-specific nature of plant morphology, which adds further complexity to the quantification of vegetative flow resistance (Aberle and Järvelä, 2013; Folkard, 2011b; Green, 2006; Kouwen and Unny, 1973).

In vegetated flows, the canopy is defined as the above ground part of the plant stand consisting of all branches, stems, leaves and stipes (Paul *et al.*, 2014). One approach to define canopy geometry is based on the size of the individual stems and blades, and the number of these elements per bed area (Nepf, 2012a). It is assumed that if the canopy elements have a characteristic diameter, d, and an average spacing between elements, ΔS, then the frontal area per canopy volume is $A = d/\Delta S^2$. For foliated vegetation types, this is defined as the leaf area index (e.g., Kaimal and Finnigan, 1994) and when integrated over the plant height, the canopy density (λf) is predicted from the frontal area per bed area, also known as the roughness density (Wooding *et al.*, 1973). However, aquatic canopies exhibit a wide range of morphologies and densities (Leonard and Luther, 1995; Lightbody and Nepf, 2006; Valiela *et al.*, 1978), with stiffer, emergent plants tending to have

rounded stems and submerged grasses tending to have a blade geometry (Nepf, 2012a). Furthermore, variations in the size, shape and density of plant elements can have a vertical dependence, which contribute towards the overall plant shape (Wilson *et al.*, 2005). In natural settings, therefore, a considerable range of vegetation morphologies exist.

This is further complicated where branches and leaves add to the total surface area, therefore creating a greater obstacle to flow than the plant stem alone (Leonard and Luther, 1995). Within the vegetation canopy flow is forced around each branch or leaf so that the velocity field is spatially heterogeneous at the scale of these elements. Vegetation structure, in particular the vertical and horizontal distribution of biomass, is therefore reported to control flow through, over and around vegetation layers (Tempest *et al.*, 2015). Furthermore, the velocity and driving forces within a submerged canopy has a range of behaviour depending on the relative depth of submergence (Nepf and Vivoni, 2000), defined as the ratio of flow depth, H, to canopy height, h. In lowland river systems most submerged aquatic canopies occur in the range of shallow submergence $H/h<5$ (Chambers and Kaiff, 1985; Duarte, 1991), for which both turbulent stress and potential pressure gradients are important in driving flow over the canopy.

Our current understanding of flows through shallow submerged vegetation comes from physically scaled flume models, field studies, and numerical modelling studies. Flume models have been used to provide a process-based understanding of complex canopy flows, and the drag processes that contribute towards the development of a mean velocity profile often described and approximated as S-shaped, or inflected (Nepf, 2012b). The representation of the vegetation in these laboratory experiments is crucial, with vegetation generally represented by: (i)

artificial plants or surrogates, or (ii) scaled plants or natural plants (Frostick *et al.*, 2011).

At the simplest level, discrete, rigid cylindrical elements arranged in varying spatial configurations have been used to represent specific attributes such as stem density in stiff, emergent plants (Liu *et al.*, 2008; Nepf, 1999). Conversely, polyethylene strips have been used to represent the flexibility and reconfiguration commonly observed in shallowly submerged species e.g. Mediterranean seagrass *Posidonia oceanica* (Folkard, 2005; Folkard, 2011a). To replicate realistic structural distributions of natural plants, artificial surrogates with an explicit parameterisation of biomass have recently been used (Schoneboom *et al.*, 2010). Often, however, artificial representations of vegetation neglect the horizontal and vertical variation in plant structure observed in the natural prototype habitat, which can lead to the incorrect predictions of flow at the plant and canopy scale (Tempest *et al.*, 2015). Where natural vegetation is used (Järvelä, 2002; Sand-Jensen, 2003; Siniscalchi and Nikora, 2012), samples can prove difficult to maintain under laboratory conditions and may not capture the variety of characteristics observed in vegetation (Frostick *et al.*, 2011). Misrepresentation of artificial or real vegetation morphology would be translated into the flow field, and any simplification may therefore compromise the representativeness of results, where alterations to the velocity and pressure fields will have primary implications for the calculation of vegetative flow resistance.

Field studies add further to our understanding, with the collection of three-dimensional velocity fields around large woody debris (Daniels and Rhoads, 2003), and isolated patches of in-situ submerged macrophytes (Schoelynck *et al.*, 2013). Furthermore, the turbulence structure has been investigated around

heterogeneously distributed submerged macrophytes (Sukhodolov and Sukhodolova, 2010), and tree-centred emergent bars (Sukhodolov and Sukhodolova, 2014). Although these studies provide great detail of the flow field, an adequate quantification of the structure of the vegetation can prove difficult.

In high dimensional numerical modelling, vegetation has been represented by adding a drag-related bulk source and sink term into the continuity equation (Fischer-Antze *et al.*, 2001; López and García, 2001). The drag force term is based on plant density and an assumed rigid, cylindrical representation of vegetation, with a drag coefficient of unity which is applicable for rigid cylinders with Reynolds numbers between $1x10^3$ - $2x10^5$ (Cheng, 2013; Panton, 1984). These models reproduce mean and turbulent flow, although they do not effectively predict the quantitative detail of turbulence namely shear and wake scales (Defina and Bixio, 2005). Such an approach has been further developed by dividing the drag into stem drag and leaf drag (Yue *et al.*, 2007), where stem drag was modelled as above, but leaf drag was modelled separately using an estimated leaf area index. An alternative approach is to include individual vegetation stems. Stoesser *et al.* (2009, 2010) included an array of individually represented rigid cylinders using Large Eddy Simulation, and by using a fine grid ensured that drag was directly accounted for, removing the need for empirical drag coefficients. Several studies have sought to incorporate flexible vegetation canopies. Ikeda *et al.* (2001) developed a biomechanical plant model based upon the dynamic Euler-Bernoulli cantilever beam equation within a two dimensional LES framework. Marjoribanks *et al.* (2014c) developed a similar model within a three-dimensional LES framework to look at arrays of semi-rigid stems within flows. Similar approaches have been developed for highly flexible vegetation applying a N-pendula equation (e.g. Abdelrhman, 2007; Dijkstra and Uittenbogaard,

136 2010). However, in all of these approaches each plant is represented as a single
137 stem and does not incorporate the complex plant morphology.

138 Here we report on a new methodology to incorporate a complex plant morphology
139 into a numerical model used to predict flow-vegetation interactions. We model the
140 three-dimensional velocity and pressure fields, at a high spatial resolution, around an
141 isolated laboratory plant stand. The plant is characterised by a complex morphology,
142 having a natural stem and leaf distribution. We model the flow around both a foliated
143 and defoliated representation of the plant, following manual removal of the foliage.
144 For this initial proof of concept work, a single plant stand has been selected to better
145 quantify the plant structure, and ensure any differences in the flow response can be
146 attributed to the different foliation states, therefore enabling the resistance effects of
147 the leaf body to be quantified.

148 We describe a physically-based characterisation of vegetation using terrestrial laser
149 scanning (TLS) which is subsequently incorporated into a computational fluid
150 dynamics (CFD) model by application of a mass flux scaling algorithm (Hardy *et al.*,
151 2005). Application of TLS enabled a three-dimensional model of the vegetation to be
152 rapidly captured into a Cartesian digital framework; that was subsequently
153 incorporated into numerical discretisation. For the first time, the morphological
154 complexity of the vegetation is then directly represented within the CFD model,
155 enabling a high resolution prediction of the three-dimensional velocity and pressure
156 fields, and the improved estimation of the drag force acting on the plant. The wider
157 implications for flow and sediment transport modelling around morphologically
158 complex vegetation, and future methodological developments, are discussed.

Methodology:

Terrestrial Laser Scanning (TLS) and voxelisation

TLS has been used to acquire a three-dimensional representation of *Prunus laurocerasus*, an invasive species to the United Kingdom increasingly recorded in riparian zones. The evergreen shrub can reach heights of 6 m, with large (0.05-0.18 m) oblong-acute, glossy, dark-green leaves and pale green branches (Polunin and Everard, 1969; Stace, 2010). *Prunus laurocerasus* was selected for scanning given its complex branch and leaf structure, and its ability to survive in laboratory conditions for prolonged periods. The woody shrub shares morphological similarities to woody riverine vegetation species such as *Populus nigra*, typically found on gravel bars (O'Hare *et al.*, 2015). In this application, a RIEGL VZ-1000 scanner was used in a controlled laboratory environment. The scanner has a beam divergence of 0.3 mrad, a field of view 100° x 360° and an effective measurement rate of up to 122 000 measurements per second. Scans were collected at a distance of 3 m, with π and θ increments set to 0.012 degrees, controlling the horizontal and vertical alignment respectively. Riegl (2015) report that at a distance of 10 m, the scanner has a range accuracy of 8 mm, and a precision of 5 mm. The scanner recorded multiple discrete returns from a single emitted pulse, improving the interrogation of vegetation elements (Pirotti *et al.*, 2013), thereby heightening point density. To resolve issues of occlusion, scans were acquired from four different perspectives to provide the requisite overlap to capture the full three-dimensionality of the plant morphology (Moorthy *et al.*, 2008).

Scans were completed under foliated and defoliated states, following manual removal of leaves (n = 432) (See Fig. 1). Individual point clouds were registered

183 using georeferenced reflective targets in RiSCAN PRO, supplemented by multi-
184 station adjustment. Similar to the workflow of Jalonen *et al.* (2015) post-processing
185 was completed using CloudCompare software. After delineation of the area of
186 interest, erroneous data points were filtered using a statistical outlier removal tool
187 (SOR). The distance-weighted filter removed isolated points on the plant surface,
188 specifically those off-centre hits caused by the position and size of the laser pulse
189 footprint relative to the feature being scanned (Béland *et al.*, 2014). By calculating
190 the mean distance between each point in the initial point cloud and a neighbourhood
191 of its nearest points, and assuming a Gaussian distribution, those points which fall
192 outside of a defined standard deviation threshold are regarded as outliers and
193 removed (Rusu *et al.*, 2008). Following Jalonen *et al.* (2015), we calculate the mean
194 distance between every point and its 100 nearest neighbours, and remove those
195 points which fall outside of 1 standard deviation from the mean. Point clouds visually
196 match the actual plant morphology (Fig. 1a), containing ≈3 500 000 points in the
197 foliated state (Fig. 1b), and ≈1 000 000 points in the defoliated state (Fig. 1c). A
198 characteristic subsection of the plant, (Fig. 1b and 1c), has been incorporated into
199 the numerical model. This subsection shares the same morphological
200 characteristics (e.g. branch thickness, leaf density) as the remainder of the plant, but
201 allows flow to be solved at a higher spatial resolution in the modelling domain (see
202 below).

203 The millimetre scale spatial resolution of this point cloud exceeded what could
204 feasibly be discretised within the CFD model, owing to the computational expense
205 associated with solving flow at such high spatial resolutions. A simplification
206 procedure following the gap fraction method of Straatsma *et al.* (2008) was applied,
207 with subdivision of the scan into individual voxels (Béland *et al.*, 2011).

Morphological properties of vegetation have previously been established using either spherical voxels (e.g., Antonarakis *et al.*, 2010) or cubic voxels (e.g., Durrieu *et al.*, 2008), however given the Cartesian grid structure of the CFD domain (see next section), a cubic voxel representation was used. Voxelisation involved the fitting of an octree structure with a user-defined maximum cell size (0.01 m) around the point clouds, which captured the morphological complexity of the plant in both defoliated and foliated states. The voxel size was justified given the branch diameter was in the range 0.01-0.1 m, and therefore the voxel size closely approximated the finest morphological elements. The voxelisation process is summarised for a subsample of the defoliated and foliated scans (Fig. 1b and 1c), outputting *XYZ* cell centroid coordinates that are read directly into the CFD discretisation (see Fig. 2).

The numerical model

The numerical scheme involves a finite volume solution of the full three-dimensional Navier-Stokes equations in a Cartesian coordinate system, with a Renormalized Group Theory (RNG) k-ε turbulence model. The closure model is applied given the large degree of fluid strain associated with flow around the plant as the RNG k-ε turbulence model calculates diffusion across the spectrum of scales (Yakhot and Orszag, 1986). A hypothetical domain 350 cells long, 120 cells wide and 100 cells high (4 200 000 grid cells) was created at a spatial resolution of 0.01 m. The numerical simulations are run until the convergence criteria is met which is dependent upon the mass conservation and momentum errors. In this application the convergence criterion was set such that mass and momentum flux residuals were reduced to 0.1% of the inlet flux.

A static representation of the plant, through the voxelised blockage, was represented using the Mass Flux Scaling Algorithm (MFSA) (Hardy *et al.*, 2005; Lane *et al.*, 2002; Lane *et al.*, 2004). The MFSA has previously been used to represent flow over complex topography such as gravel surfaces (Hardy *et al.*, 2007), and idealised single stemmed vegetation elements that are used to represent a vegetation canopy (Marjoribanks *et al.*, 2014c). The MFSA represents the plant as a numerical porosity, and enables the voxelised plant to occupy a specified fraction of each grid cell. For each grid cell a binary occupied/unoccupied porosity is defined because the 0.01 m voxel size is equal to that of the 0.01 m grid cell size. The voxelised blockage was incorporated 0.5 m downstream from the inlet (0.14 *X/l*), and centred (0.5 *Y/w)*. The bed was treated as a nonslip boundary using the logarithmic law of the wall and domain side walls were considered frictionless boundaries. The vegetation-flow interface is treated as an immersed boundary. Inlet conditions are held constant between the defoliated and foliated model runs with the downstream velocity set to 0.25 m s^{-1} with an inlet turbulent intensity of 5%. Thus, the flow was assumed to be fully turbulent and subcritical. The outlet was defined using a fixed-pressure boundary condition where mass is allowed to enter and leave the domain.

Results:

Here we present the downstream (*u*-component) velocity field for the defoliated and foliated cases (Fig. 2c and 2f) in plan view at 0.4 and 0.6 *Z/h* (Fig. 3a and 4a). Under the defoliated state (Fig. 3a), individual stems introduce flow separation and reattachment with the formation of narrow wakes of reduced velocity. At 0.4 *Z/h*, coalescence of these wakes is observed. However, this behaviour varies vertically, and at 0.6 *Z/h*, where the branches are spaced further apart, wakes behave independently. Wake coalescence would therefore depend on the separation distance between individual branches. Under the foliated scenario (Fig. 4a), a single, more pronounced zone of flow separation and reattachment is evident, indicative of behaviour shown by a bluff object. In the foliated state, the shape of the wake is vertically non-uniform, which is a function of the vertical and lateral distribution of the plant morphology, and results in flow asymmetry. For example, at 0.4 *Z/h* the abundance of leaves at lower *Y/w* values produce an asymmetrical wake structure that extends further downstream than the corresponding wake in the defoliated state. For both the defoliated and foliated states similarities can be observed; namely a reduction in velocity immediately upstream of the blockage, with marginal flow acceleration around the blockage edges, indicative of flow in a junction vortex system (Simpson, 2001). It is suggested that this canopy shear layer turbulence is dominated by Kelvin-Helmholtz and Görtler-type vortices generated through shear instability, which evolve with distance downstream of the plant (Ghisalberti and Nepf, 2002).

The wake shape is further illustrated through a vertical slice down the midline (0.5 *Y/w*) (Fig. 3b and 4b). In both cases, wake shape varies considerably with *Z/h*. For the defoliated state, development of a wake zone at 0.2-0.4 *Z/h* corresponds with the

main branching point of the plant (see Fig. 2), with a concentration of branches. The wake is inclined slightly upwards, thins in the downstream direction and extends ≈7 plant lengths downstream. Marginal flow acceleration is evident around the outer edge of the central branch. A more complex wake structure consisting of two discrete layers is evident in the foliated state. Again, the lower wake corresponds with the branching point at 0.2-0.4 *Z/h*, although only extends ≈3 plant lengths downstream. Above this, a pronounced and thicker wake zone at 0.45-0.65 *Z/h* corresponds with the dense foliation, and extends ≈7 plant lengths downstream. The dense foliation component is influential in producing a localised velocity response.

The morphological complexity of the plant introduces additional flow heterogeneity, therefore velocity profiles begin to deviate from the idealised inflected profiles that are associated with canopy flows (Fig. 5a, inset graph). Fig. 5 provides evidence for three distinct velocity zones in the vertical, namely: a zone of relative flow acceleration beneath the bulk of the plant in the near bed region (sub-canopy flow), a zone of flow acceleration above the plant in the free stream zone, and between these a non-uniform low velocity zone associated with flow deceleration around the plant blockage. The shape of the vertical velocity profiles clearly differ between the defoliated and foliated states. When defoliated, the velocity minima is positioned lower in the flow depth, and associated with the point at which the main branch splits into sub-branches (see Fig. 2). When foliated, however, the velocity minima is shifted higher in the flow, and associated with the main leaf body. The magnitude and size of the low velocity zone in the foliated state is exaggerated relative to the defoliated state, illustrating the important role of the leaf body in modifying the flow disturbance. In both foliation states the accelerated sub-canopy flow component appears to be similarly sized and shaped, indicating that distance between the bed

298 and base of the main plant blockage influences the characteristics of this zone. The
299 velocity profiles show that with increasing distance downstream, the flow begins to
300 recover, with velocity profiles becoming more modulated, and velocities reverting
301 towards the inlet velocity of 0.25 m s^{-1}.

302 Especially in the foliated state proximal to the blockage (Fig. 5a and Fig. 5b), a sharp
303 transition is evident between the reduced velocity zone and free stream zone,
304 characterised by flow acceleration, with this velocity discontinuity indicative of shear
305 layer formation and the presence of Kelvin-Helmholtz instabilities (Ghisalberti and
306 Nepf, 2002). The shear layer appears more prominent where the plant thickness is
307 larger and therefore the shear layer scales with the local plant thickness. Vortex
308 growth stops when turbulent energy production is equal to dissipation (Ghisalberti
309 and Nepf, 2004).

310 At the wake scale, mean kinetic energy is converted into wake-generated turbulent
311 kinetic energy at the scale of the plant stems (Ghisalberti and Nepf, 2002) and
312 therefore analysis of the turbulent kinetic energy (TKE) provides an estimation of the
313 amount of form drag introduced by the plant (Raupach and Shaw, 1982). Direct
314 comparisons between the defoliated and foliated states are shown at 0.45 *Z/h* (Fig.
315 6a and 6b). In both cases, zones of high TKE (> 0.04 m^2/s^2) are observed proximal
316 to the outer edge of the plant, driven by the forcing of flow around the blockage,
317 resulting in flow acceleration (*u*-component) and lateral movement (*v*-component).
318 For the defoliated state, these high TKE zones are enclosed around individual
319 branches, whereas in the foliated state the zones are comparably larger and extend
320 a greater distance from the vegetation front, due to a longer, more pronounced
321 disturbance to the *v*-component of velocity. Because of the complex, interacting

322 nature of the wakes in the defoliated state, the leeward zone of low TKE (< 0.015
323 m^2/s^2) is more fragmented and extends a greater distance downstream than in the
324 foliated state. Again this demonstrates canopy shear layer instability, dominated by
325 Kelvin-Helmholtz and Görtler-type vortices evolving with distance downstream of the
326 plant.

327 Pressure fields are analysed to calculate the drag force and subsequent drag
328 coefficients acting on the plant (Marjoribanks, 2013). Fig. 7a and 7b show the
329 pressure fields at 0.45 *Z/h*. When defoliated, the high pressure zone located directly
330 upstream of the blockage is isolated about individual branches. When foliated,
331 however, this zone has coalesced to form a comparatively larger, single body
332 characterised by higher pressures. Similarly, downstream of the plant, isolated
333 zones of low pressure are associated with individual branches when defoliated,
334 compared with a much more pronounced and extended low pressure zone when
335 foliated.

Calculation of drag forces

The drag force is calculated by integrating the difference in the pressure field acting normal to the vegetation surface over the entire lateral extent of the plant. We sum the difference in pressure from immediately upstream and downstream of the plant. This is achieved by applying a mask to the three-dimensional vegetation extent, and extracting pressure values from one cell upstream and one cell downstream of the mask:

$$F_d = \int_A (p_f - p_b) dA \quad (1)$$

where F_d is the drag force (N/m^2), p_f is the pressure at the blockage front (Pa), p_b is the pressure at the blockage back (Pa), and A is the frontal area (m^2). In this instance where the plant is represented by a 0.01 m voxel size, this gives a cell area of 0.0001 m^2. To calculate the plant frontal area, we count the number of cells at the blockage front, and multiply this by the cell area. A full discussion of the drag calculation is provided by Marjoribanks *et al.* (2014b). Drag forces of 0.15 N/m^2 and 1.74 N/m^2 are calculated for the defoliated and foliated states respectively. This order of magnitude difference is attributed to the influence of the additional morphological complexity introduced by leaf elements, which result in a different flow response as drag increases with foliage density (Wilson *et al.*, 2003). As previously observed, leaves are shown to introduce a second wake structure that extends ≈7 plant lengths downstream, resulting in a more spatially heterogeneous velocity field. This corresponds with the more pronounced TKE patterns observed in the foliated case, indicating a greater form drag contribution. Both of these factors result from the greater number of blocked cells in the foliated state, imparting a greater

disturbance on the flow. The drag force values are of a similar order of magnitude to the direct measurements of vegetative drag force (≈0-10 N/m^2), for small natural woody trees, undertaken by Jalonen and Järvelä (2014).

Drag forces are used to calculate a drag coefficient, following:

$$C_d = \frac{F_d}{\frac{1}{2}\rho u^2 A} \quad (2)$$

where C_d is the drag coefficient, ρ is the density (kg/m^3), and u is the inlet velocity (m s^{-1}). Drag coefficients are well understood for simple geometric shapes (e.g. cylinders), but are less well understood for the complex geometries associated with natural vegetation (Marjoribanks *et al.*, 2014a). Modelling studies typically assign a drag coefficient value of unity for vegetation, however this is only applicable to the simplest reed and grass type plants. A value of unity is true for a single cylinder with Reynolds numbers between 1x10^3 - 2x10^5, although deviates significantly for more complex vegetation as it is a function of both vegetation density and stem Reynolds number (Tanino and Nepf, 2008). For sparsely configured leafy shrub communities, the flume experiments of Hui *et al.* (2010) report drag coefficients of up to 4. Here, we calculate drag coefficients of 1.54 and 1.24 for the defoliated and foliated states respectively, exceeding the typically assumed value of 1. An inverse trend between drag force and drag coefficient is surprising given the drag coefficient in the defoliated case is higher, when the drag force is an order of magnitude lower than the foliated case. This discrepancy can be explained by morphological differences. Namely, the dominance of individual branches in the defoliated state, compared to the dominance of a single leaf body of the foliated state, where sheltering effects reduce the imposed resistance on the downstream end of the plant.

Discussion and potential applications:

Analysis of downstream velocity, turbulent kinetic energy and pressure field simulations have demonstrated the importance of explicitly representing the morphological complexity of plants in the numerical description of flow in vegetated channels. The vertical and lateral distribution of the plant morphology is shown to form canopy shear layer turbulence, likely to be dominated by Kelvin-Helmholtz and Görtler-type vortices, which evolve downstream of the plant (Ghisalberti and Nepf, 2002). The approach provides a high resolution, spatially distributed set of modelled hydraulic data which can provide the framework for evaluating turbulence-vegetation-energy loss relationships, and in particularly a means for calculating drag coefficients for individual plant species.

The ability to incorporate morphologically complex vegetation into a numerical scheme has major implications for the modelling of flow, sediment transport and the associated evolution of vegetated and partially-vegetated near surface landscapes. When modelling flow, the approach better allows us to understand the flow disturbance introduced by vegetation, providing a full flow field simulation of the three-dimensional velocity and pressure fields. This extends beyond the work of Manners *et al.* (2013), who used a vertically averaged two-dimensional model around stands of *Tamarix spp*. We show that the vertical and lateral position of the vegetation, specifically the distribution of the main body of the foliage, results in a complex velocity field, and this directly influences the shape of the vertical velocity profile. Therefore across different species, it is likely that the distribution of foliage will be significant in controlling the flow patterns observed. For shrubs with an open area beneath the primary leaf mass, Freeman *et al.* (2000) demonstrated that flow is significantly diverted beneath the canopy, with an acceleration of the sub-canopy

405 flow. Similar velocity profiles were noted in field studies of flow around natural
406 willows by Bölscher *et al.* (2005). In this paper we have successfully modelled
407 similar velocity profiles (Figure 5), and this sub-canopy flow component will have
408 direct implications for elevated bed shear stresses around the plant and for surface
409 scour. When modelling flow around woody vegetation types, consisting of both a
410 branch and foliage component, there is a clear need to accurately represent this
411 morphological complexity. An over-simplified representation (e.g. a simple cylinder)
412 would fail to capture the full complexity of flow field, omitting key features such as the
413 sub-canopy flow, as well as the structure of wake shape. Järvelä *et al.* (2006)
414 specify that for predicting erosion and sediment transport, a three-dimensional
415 modelling solution that can adequately model the turbulent flow field is needed. Our
416 approach meets these demands, and therefore has potential for modelling sediment
417 transport dynamics. Crucially, we are developing the method to include a digital
418 elevation representation of the bed, which is coupled to a sediment routing model,
419 thereby offering the ability to model vegetation-flow-sediment interactions
420 simultaneously. This development will allow sediment particles to be tracked around
421 vegetation, and the patterns of local scour and deposition to be mapped.

422 However, the results presented here describe only a static representation of a single
423 plant morphology. Aquatic vegetation is seldom found in isolation (Sand-Jensen and
424 Madsen, 1992), and as such the forces on individual plants can be reduced due to
425 sheltering and through the reduced velocities in wakes from upstream plants.
426 Furthermore, flow forcing will cause foliage reconfiguration through streamlining,
427 which will subsequently reduce the drag. This has been shown to be more important
428 in drag reduction than stem bending and enables plant survival through either static
429 or dynamic reconfiguration (Nikora, 2010; Usherwood *et al.*, 1997). These

reconfiguration processes occur over a range of spatial scales from individual leaves to entire plant-patches (Albayrak *et al.*, 2013; Sand-Jensen, 2003), and therefore an explicit representation of changes to plant posture through time is also essential. Work is therefore currently underway to develop a dynamic approach that accounts for multiple dynamic, morphologically complex plants, incorporating reconfiguration and subsequent form drag reduction by developing further the approach of Marjoribanks *et al.* (2014c). This involves applying a time-varying biomechanical model coupled with Large Eddy Simulation (LES) to predict plant motion through time.

Recent experimental work has shown how the interaction of neighbouring emergent vegetation patches can influence deposition dynamics (Meire *et al.*, 2014). This has been extended into a numerical scheme, where de Lima *et al.* (2015) used CFD to show that patch distributions and interactions may be responsible for the feedbacks that influence the evolution of vegetated landscapes at the channel scale. However, in both examples vegetation is represented by cylinders of varying densities. Developing an approach which includes multiple, dynamic representations of morphologically complex plants derived from TLS will allow sediment dynamics to be further explored. Furthermore, the approach we propose is not limited to woody species associated with riverine settings, it is possible to apply the methodology to a vegetated estuarine environment where sediment dynamics are of critical importance.

Acknowledgements:

Richard J. Boothroyd was funded under NERC Doctoral Scholarship 1313876. Data used in this manuscript can be obtained by contacting the lead author. We are grateful to the Editor and two anonymous referees for providing helpful comments that have led to significant improvements in this manuscript.

Figures:

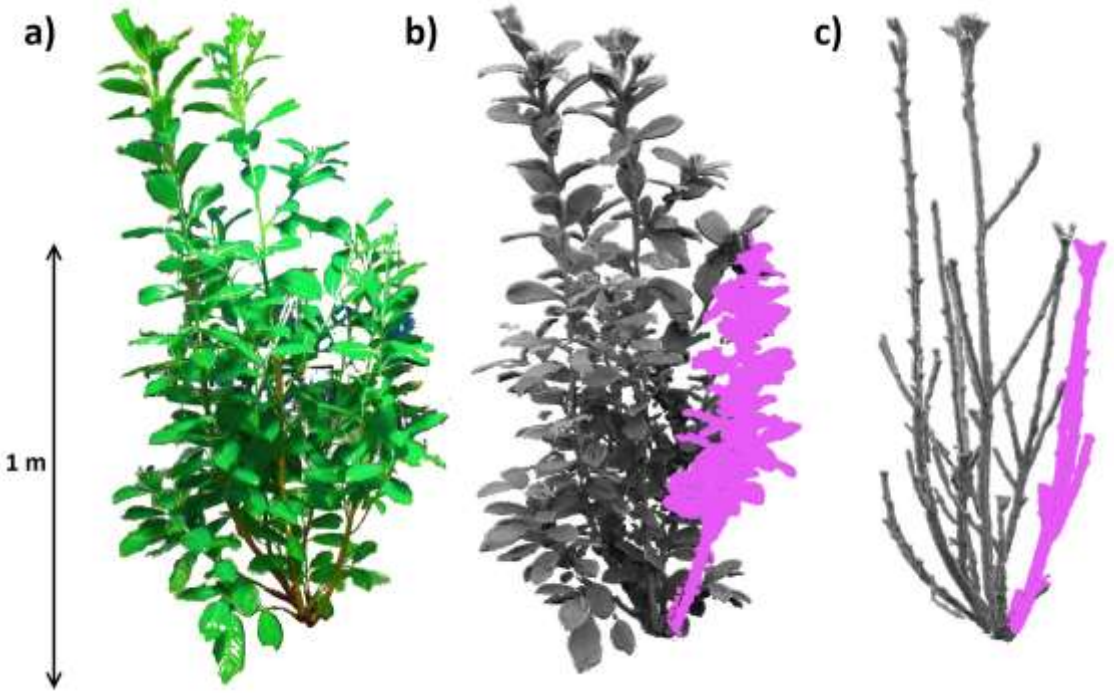

Figure 1: Three-dimensional point cloud of *Prunus laurocerasus captured using TLS*: (a) photograph in foliated state, (b) post-processed foliated point cloud with subsection used in numerical model highlighted (Fig. 2), (c) post-processed defoliated point cloud, following manual removal of leaves (n = 432), with characteristic subsection highlighted (Fig. 2).

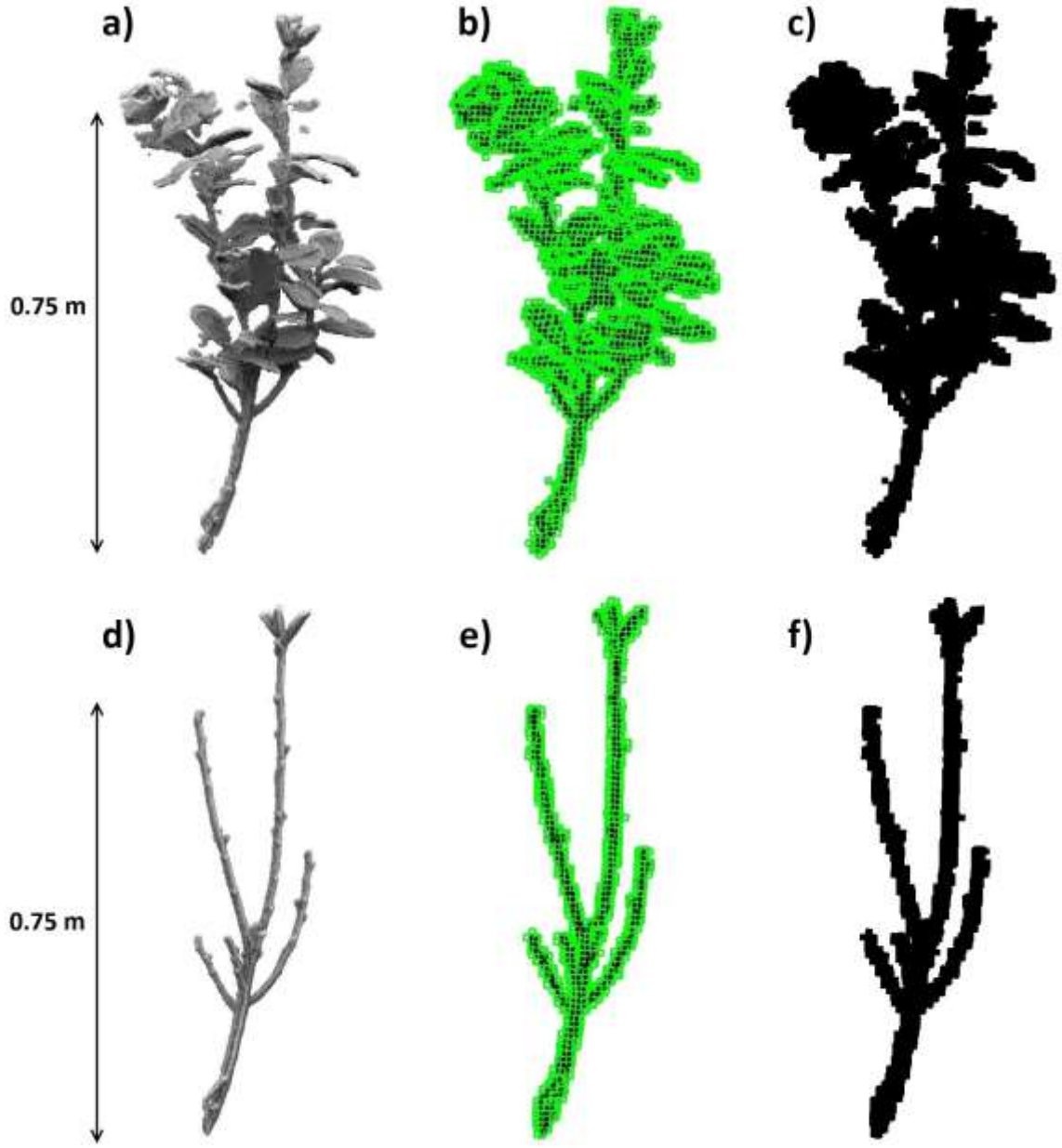

465

466 **Figure 2:** Stages of the voxelisation process, for the foliated (a-c) and defoliated (d-f)
467 subsections: (a and d) illustrate the post-processed point cloud; (b and e) the user-
468 defined octree structure with a cell size of 0.01 m fitted around the point cloud; and
469 (c and f) the voxelised representation, following extraction of *XYZ* coordinates of
470 octree centroids.

471

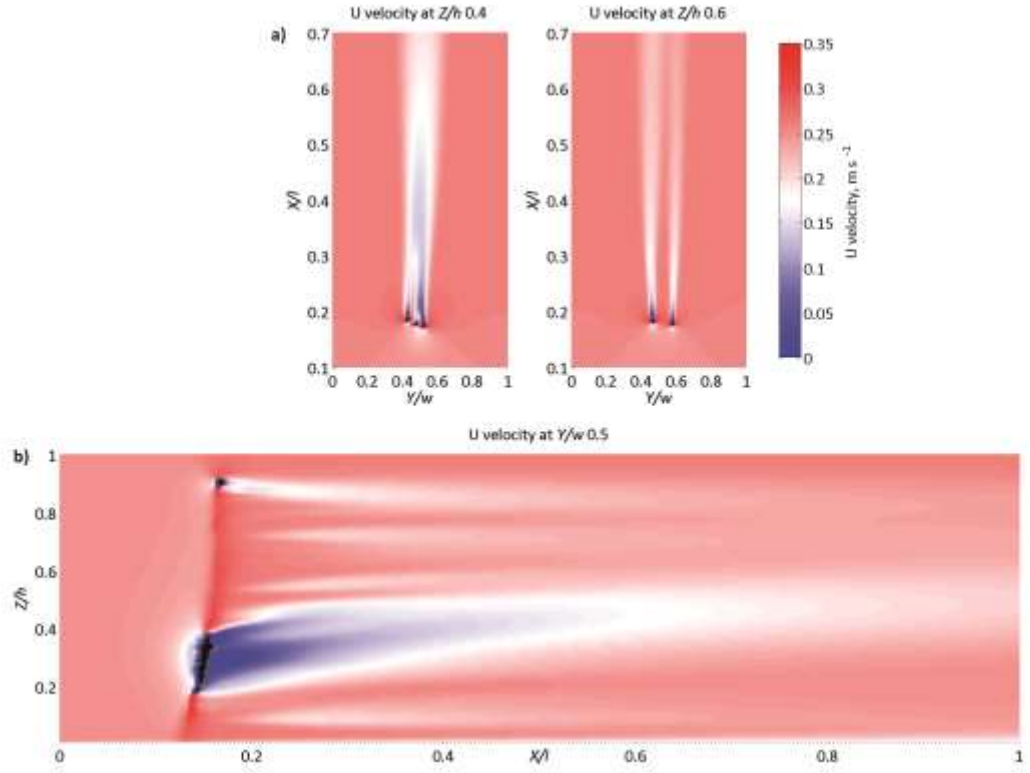

472

473 **Figure 3:** Downstream (*u*-) velocity field data for the defoliated state: (a) slices at 0.4
474 and 0.6 *Z/h*. The position of the plant is marked as the solid black region.
475 Downstream wakes can coalesce or act independently from one another, based on
476 the separation distance of individual branches. (b) Vertical slice taken at the midline
477 (0.5 *Y/w*), where a spatially non-uniform wake shape in the vertical dimension is
478 shown. The wake zone at 0.2-0.4 *Z/h* is associated with the main branching point,
479 and extends ≈7 plant lengths downstream.

480

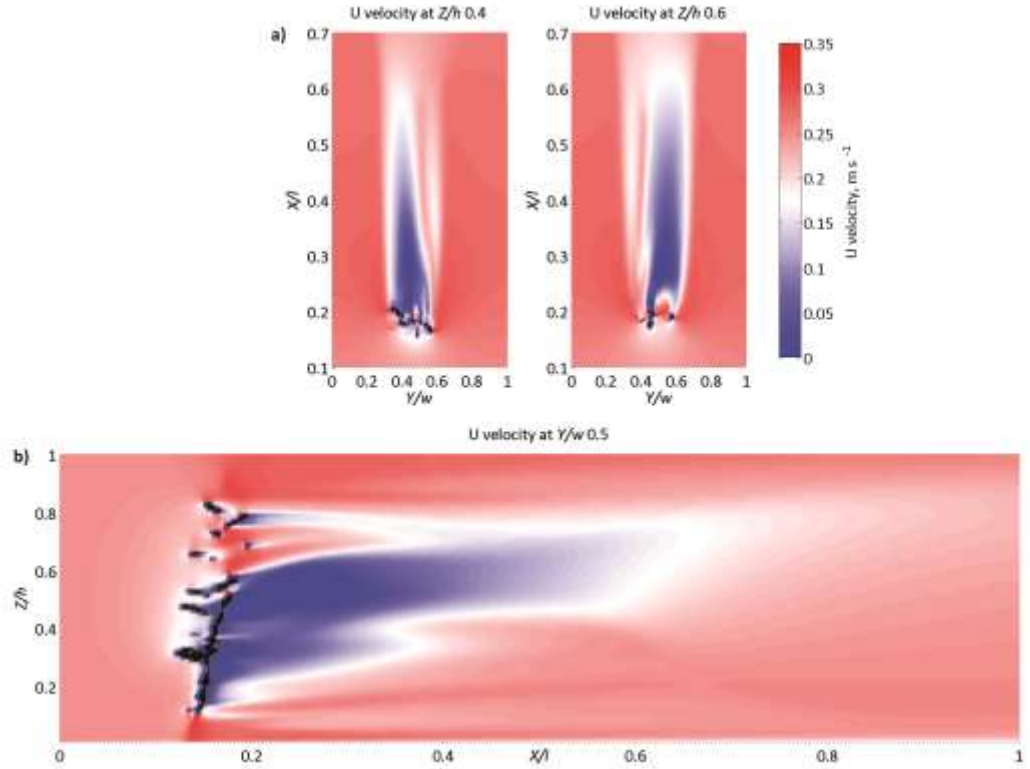

481

482 **Figure 4:** Downstream (*u*-) velocity field data for the foliated state: (a) slices at 0.4
483 and 0.6 *Z/h* show a single, more pronounced zone of flow separation and
484 reattachment, indicative of behaviour shown by a bluff object. (b) Vertical slice taken
485 at the midline (0.5 *Y/w*) illustrates two discrete wakes. Similarly to the defoliated
486 case, the lower wake corresponds with the branching point at 0.2-0.4 *Z/h* although
487 only extends ≈3 plant lengths downstream. Above this, a more pronounced wake at
488 0.45-0.65 *Z/h* corresponds with the bulk of the leafy blockage, extending ≈7 plant
489 lengths downstream. The leafy component has a first order control on the
490 production of a spatially heterogeneous velocity field.

491

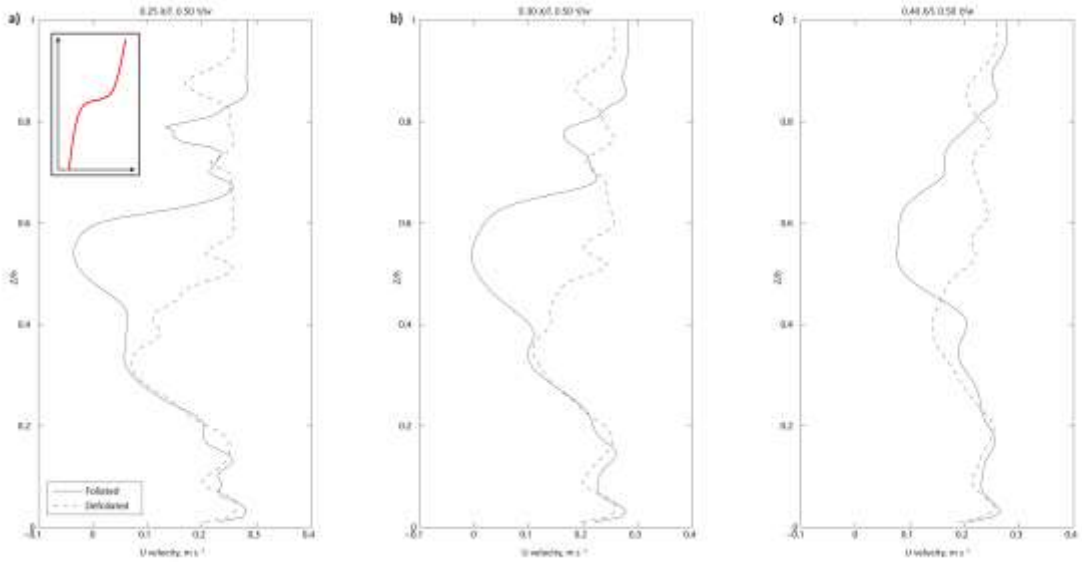

492

493 **Figure 5:** Vertical velocity profiles extracted from the midline (0.5 *Y/w*) at increasing
494 distances downstream: (a) 0.25 *X/l*, (b) 0.30 *X/l*, (c) 0.40 *X/l*. The inset graph in (a)
495 illustrates an idealised inflected velocity profile often used to characterise vegetated
496 flows. The velocity profiles illustrate the complex vertical structure in the wake of the
497 flow. Three velocity zones are identified, namely: a zone of relative flow acceleration
498 beneath the bulk of the plant in the near bed region (sub-canopy flow), a zone of flow
499 acceleration above the plant in the free stream zone, and between these, a non-
500 uniform low velocity zone associated with flow deceleration due to the bulk of the
501 plant blockage. The magnitude and size of the low velocity zone is exaggerated in
502 the foliated state, where the leaf body acts to further decelerate flow in the wake.

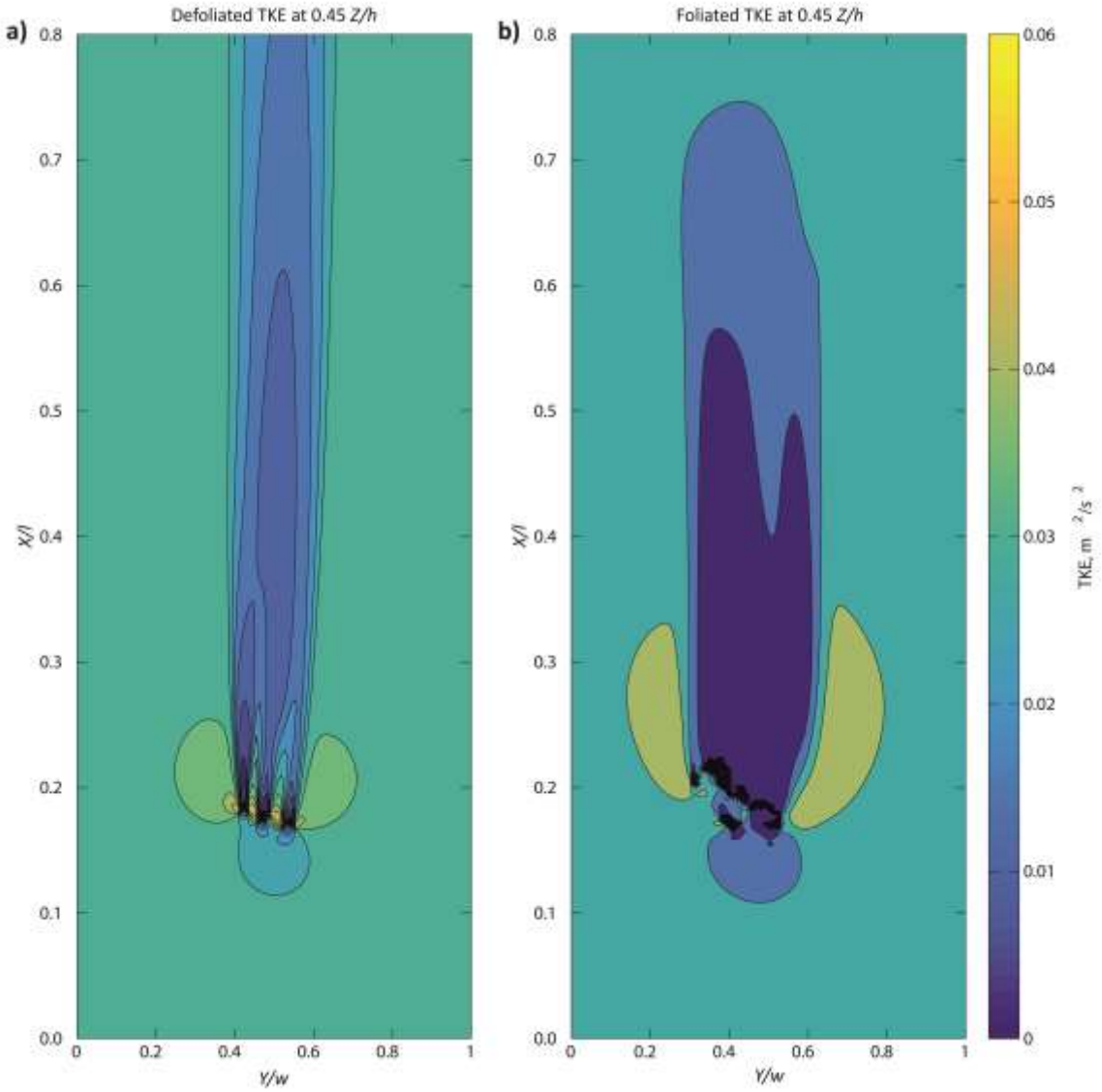

503

504 **Figure 6:** Turbulent Kinetic Energy (TKE) for (a) defoliated and (b) foliated
505 scenarios, 0.45 *Z/h*. In both cases, a zone of high TKE (> 0.04 m^2/s^2) is evident
506 proximal to the outer edge of the vegetation. In the defoliated scenario, this is
507 enclosed by a slightly lower zone of TKE (0.03-0.04 m^2/s^2), whereas in the foliated
508 scenario, the high TKE zone is larger, and persists in the downstream direction.
509 Overall, TKE patterns indicate a greater form drag contribution in the foliated case.

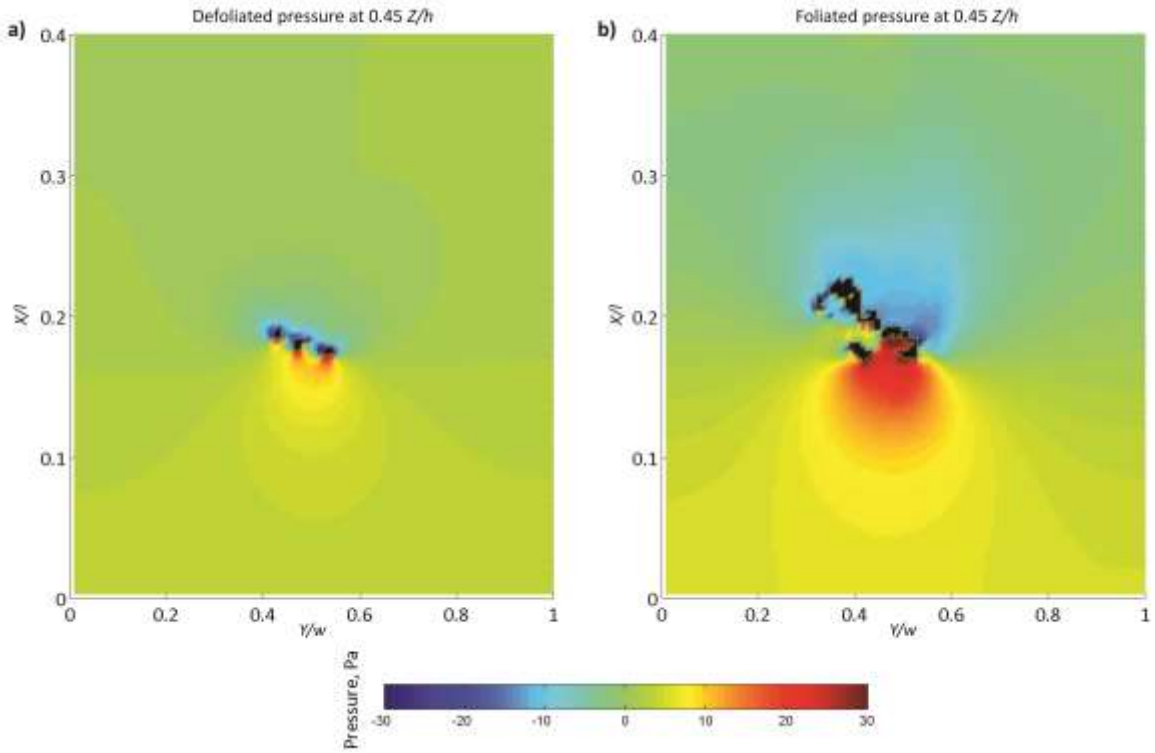

Figure 7: Pressure fields at 0.45 *Z/h* for: (a) the defoliated state, where individual branches cause the formation of isolated zones of high pressure upstream, and low pressure downstream. (b) The foliated state exhibits different behaviour, with the formation of a more pronounced zone of high pressure upstream, and coalescence of the low pressure zone downstream; again indicative of bluff behaviour.

References:

Abdelrhman MA. 2007. Modeling coupling between eelgrass Zostera marina and water flow. Marine Ecology Progress Series **338**: 81-96. DOI: 10.3354/meps338081

Aberle J, Järvelä J. 2013. Flow resistance of emergent rigid and flexible floodplain vegetation. Journal of Hydraulic Research **51**: 33-45. DOI: 10.1080/00221686.2012.754795

Albayrak I, Nikora V, Miler O, O'Hare M. 2013. Flow–plant interactions at leaf, stem and shoot scales: drag, turbulence, and biomechanics. Aquatic Sciences **76**: 1-26. DOI: 10.1007/s00027-013-0335-2

Antonarakis AS, Richards KS, Brasington J, Muller E. 2010. Determining leaf area index and leafy tree roughness using terrestrial laser scanning. Water Resources Research **46**: W06510. DOI: 10.1029/2009WR008318

Béland M, Baldocchi DD, Widlowski J-L, Fournier RA, Verstraete MM. 2014. On seeing the wood from the leaves and the role of voxel size in determining leaf area distribution of forests with terrestrial LiDAR. Agricultural and Forest Meteorology **184**: 82-97. DOI: 10.1016/j.agrformet.2013.09.005

Béland M, Widlowski J-L, Fournier RA, Côté J-F, Verstraete MM. 2011. Estimating leaf area distribution in savanna trees from terrestrial LiDAR measurements. Agricultural and Forest Meteorology **151**: 1252-1266. DOI: 10.1016/j.agrformet.2011.05.004

Bölscher J, Ergenzinger P, Obenauf PJ. 2005. Hydraulic, sedimentological and ecological problems of multifunctional riparian forest management - RIPFOR the scientific report. In *Heft 65*. Berliner Geographische Abhandlungen: Berlin; 146.

Carpenter SR, Lodge DM. 1986. Effects of submersed macrophytes on ecosystem processes. Aquatic Botany **26**: 341-370. DOI: 10.1016/0304-3770(86)90031-8

Chambers PA, Kaiff J. 1985. Depth Distribution and Biomass of Submersed Aquatic Macrophyte Communities in Relation to Secchi Depth. Canadian Journal of Fisheries and Aquatic Sciences **42**: 701-709. DOI: 10.1139/f85-090

Cheng N-S. 2013. Calculation of Drag Coefficient for Arrays of Emergent Circular Cylinders with Pseudofluid Model. Journal of Hydraulic Engineering **139**: 602-611. DOI: 10.1061/(ASCE)HY.1943-7900.0000722

Daniels MD, Rhoads BL. 2003. Influence of a large woody debris obstruction on three-dimensional flow structure in a meander bend. Geomorphology **51**: 159-173. DOI: 10.1016/S0169-555X(02)00334-3

de Lima PHS, Janzen JG, Nepf HM. 2015. Flow patterns around two neighboring patches of emergent vegetation and possible implications for deposition and vegetation growth. Environmental Fluid Mechanics **15**: 881-898. DOI: 10.1007/s10652-015-9395-2

Defina A, Bixio AC. 2005. Mean flow and turbulence in vegetated open channel flow. Water Resources Research **41**: W07006. DOI: 10.1029/2004WR003475

Dijkstra JT, Uittenbogaard RE. 2010. Modeling the interaction between flow and highly flexible aquatic vegetation. Water Resources Research **46**: W12547. DOI: 10.1029/2010WR009246

Duarte CM. 1991. Seagrass depth limits. Aquatic Botany **40**: 363-377. DOI: 10.1016/0304-3770(91)90081-F

Durrieu S, Allouis T, Fournier R, Véga C, Albrech L. 2008. Spatial quantification of vegetation density from terrestrial laser scanner data for characterization of 3D forest structure at plot level. In *SilviLaser 2008*: Edinburgh, UK; 325-334.

Fischer-Antze T, Stoesser T, Bates P, Olsen NRB. 2001. 3D numerical modelling of open-channel flow with submerged vegetation. Journal of Hydraulic Research **39**: 303-310. DOI: 10.1080/00221680109499833

Folkard AM. 2005. Hydrodynamics of model Posidonia oceanica patches in shallow water. Limnology and oceanography **50**: 1592-1600. DOI: 10.4319/lo.2005.50.5.1592

Folkard AM. 2011a. Flow regimes in gaps within stands of flexible vegetation: laboratory flume simulations. Environmental Fluid Mechanics **11**: 289-306. DOI: 10.1007/s10652-010-9197-5

Folkard AM. 2011b. Vegetated flows in their environmental context: a review. Proceedings of the ICE-engineering and computational mechanics **164**: 3-24. DOI: 10.1680/eacm.8.00006

Freeman GE, Rahmeyer WH, Copeland RR. 2000. Determination of resistance due to shrubs and woody vegetation. ERDC/CHL TR-00-25. Coastal and Hydraulics Laboratory: Vicksburg, MS.

Frostick LE, McLelland SJ, Mercer TG. 2011. Ecological experiments. In *Users Guide to Physical Modelling and Experimentation*, Frostick LE, McLelland SJ, Mercer TG (eds). CRC Press; 127-170.

Ghisalberti M, Nepf HM. 2002. Mixing layers and coherent structures in vegetated aquatic flows. Journal of Geophysical Research: Oceans **107**: 3-1-3-11. DOI: 10.1029/2001jc000871

Ghisalberti M, Nepf HM. 2004. The limited growth of vegetated shear layers. Water Resources Research **40**: W07502. DOI: 10.1029/2003WR002776

Green JC. 2006. Effect of macrophyte spatial variability on channel resistance. Advances in Water Resources **29**: 426-438. DOI: 10.1016/j.advwatres.2005.05.010

Hardy RJ, Lane SN, Ferguson RI, Parsons DR. 2007. Emergence of coherent flow structures over a gravel surface: A numerical experiment. Water Resources Research **43**: W03422. DOI: 10.1029/2006wr004936

Hardy RJ, Lane SN, Lawless MR, Best JL, Elliott L, Ingham DB. 2005. Development and testing of a numerical code for treatment of complex river channel topography in three-dimensional CFD models with structured grids. Journal of Hydraulic Research **43**: 468-480. DOI: 10.1080/00221680509500145

Hui E-q, Hu X-e, Jiang C-b, Ma F-k, Zhu Z-d. 2010. A study of drag coefficient related with vegetation based on the flume experiment. Journal of Hydrodynamics, Ser. B **22**: 329-337. DOI: 10.1016/S1001-6058(09)60062-7

Ikeda S, Yamada T, Toda Y. 2001. Numerical study on turbulent flow and honami in and above flexible plant canopy. International Journal of Heat and Fluid Flow **22**: 252-258. DOI: 10.1016/S0142-727X(01)00087-X

Jalonen J, Järvelä J. 2014. Estimation of drag forces caused by natural woody vegetation of different scales. Journal of Hydrodynamics, Ser. B **26**: 608-623. DOI: 10.1016/S1001-6058(14)60068-8

Jalonen J, Järvelä J, Virtanen J-P, Vaaja M, Kurkela M, Hyyppä H. 2015. Determining Characteristic Vegetation Areas by Terrestrial Laser Scanning for Floodplain Flow Modeling. Water **7**: 420-437. DOI: 10.3390/w7020420

Järvelä J. 2002. Flow resistance of flexible and stiff vegetation: a flume study with natural plants. Journal of Hydrology **269**: 44-54. DOI: 10.1016/S0022-1694(02)00193-2

Järvelä J, Aberle J, Dittrich A, Rauch H, Schnauder I. 2006. Flow-vegetation-sediment interaction: Research challenges. In *River Flow 2006*. Taylor & Francis: Lisbon, Portugal; 2017-2026.

Kadlec R. 1990. Overland Flow in Wetlands: Vegetation Resistance. Journal of Hydraulic Engineering **116**: 691-706. DOI: 10.1061/(ASCE)0733-9429(1990)116:5(691)

Kaimal JC, Finnigan JJ. 1994. Atmospheric boundary layer flows: their structure and measurement. Oxford University Press: New York

Kouwen N, Unny TE. 1973. Flexible Roughness in Open Channels. Journal of the Hydraulics Division **99**: 713-728

Lane SN, Hardy RJ, Elliott L, Ingham DB. 2002. High-resolution numerical modelling of three-dimensional flows over complex river bed topography. Hydrological Processes **16**: 2261-2272. DOI: 10.1002/hyp.5034

Lane SN, Hardy RJ, Elliott L, Ingham DB. 2004. Numerical modeling of flow processes over gravelly surfaces using structured grids and a numerical porosity treatment. Water Resources Research **40**: W01302. DOI: 10.1029/2002wr001934

Leonard LA, Luther ME. 1995. Flow hydrodynamics in tidal marsh canopies. Limnology and oceanography **40**: 1474-1484. DOI: 10.4319/lo.1995.40.8.1474

Lightbody AF, Nepf HM. 2006. Prediction of velocity profiles and longitudinal dispersion in salt marsh vegetation. Limnology and oceanography **51**: 218-228. DOI: 10.4319/lo.2006.51.1.0218

Liu D, Diplas P, Fairbanks JD, Hodges CC. 2008. An experimental study of flow through rigid vegetation. Journal of Geophysical Research: Earth Surface **113**: F04015. DOI: 10.1029/2008JF001042

López F, García M. 2001. Mean Flow and Turbulence Structure of Open-Channel Flow through Non-Emergent Vegetation. Journal of Hydraulic Engineering **127**: 392-402. DOI: 10.1061/(ASCE)0733-9429(2001)127:5(392)

Manners R, Schmidt J, Wheaton JM. 2013. Multiscalar model for the determination of spatially explicit riparian vegetation roughness. Journal of Geophysical Research: Earth Surface **118**: 65-83. DOI: 10.1029/2011JF002188

Marjoribanks TI. 2013. High resolution modelling of flexible submerged vegetation in rivers. Durham University; 363.

Marjoribanks TI, Hardy RJ, Lane SN. 2014a. The hydraulic description of vegetated river channels: the weaknesses of existing formulations and emerging alternatives. Wiley Interdisciplinary Reviews: Water **1**: 549-560. DOI: 10.1002/wat2.1044

Marjoribanks TI, Hardy RJ, Lane SN, Parsons DR. 2014b. Dynamic drag modeling of submerged aquatic vegetation canopy flows. In *River Flow 2014: proceedings of the International Conference on Fluvial Hydraulics*, Schleiss AJ, De Cesare G, Franca MJ, Pfister M (eds). CRC Press, Taylor & Francis Group: London; 517-524.

Marjoribanks TI, Hardy RJ, Lane SN, Parsons DR. 2014c. High-resolution numerical modelling of flow—vegetation interactions. Journal of Hydraulic Research **52**: 775-793. DOI: 10.1080/00221686.2014.948502

Meire DWSA, Kondziolka JM, Nepf HM. 2014. Interaction between neighboring vegetation patches: Impact on flow and deposition. Water Resources Research: 3809–3825. DOI: 10.1002/2013wr015070

Moorthy I, Miller JR, Hu B, Chen J, Li Q. 2008. Retrieving crown leaf area index from an individual tree using ground-based lidar data. Canadian Journal of Remote Sensing **34**: 320-332. DOI: 10.5589/m08-027

Nepf HM. 1999. Drag, turbulence, and diffusion in flow through emergent vegetation. Water Resources Research **35**: 479-489. DOI: 10.1029/1998wr900069

Nepf HM. 2012a. Flow and Transport in Regions with Aquatic Vegetation. Annual Review of Fluid Mechanics **44**: 123-142. DOI: 10.1146/annurev-fluid-120710-101048

Nepf HM. 2012b. Hydrodynamics of vegetated channels. Journal of Hydraulic Research **50**: 262-279. DOI: 10.1080/00221686.2012.696559

Nepf HM, Vivoni ER. 2000. Flow structure in depth-limited, vegetated flow. Journal of Geophysical Research: Oceans **105**: 28547-28557. DOI: 10.1029/2000JC900145

Nikora V. 2010. Hydrodynamics of aquatic ecosystems: An interface between ecology, biomechanics and environmental fluid mechanics. River Research and Applications **26**: 367-384. DOI: 10.1002/rra.1291

O'Hare MT, Mountford JO, Maroto J, Gunn IDM. 2015. Plant Traits Relevant To Fluvial Geomorphology and Hydrological Interactions. River Research and Applications. DOI: 10.1002/rra.2940

Panton RL. 1984. Incompressible Flow. John Wiley & Sons: New York

Paul M, Thomas RE, Dijkstra JT, Penning WE, Vousdoukas MI. 2014. Plants, hydraulics and sediment dynamics. In *Users Guide to Ecohydraulic Modelling and Experimentation*. CRC Press; 91-116.

Pirotti F, Guarnieri A, Vettore A. 2013. Ground filtering and vegetation mapping using multi-return terrestrial laser scanning. ISPRS Journal of Photogrammetry and Remote Sensing **76**: 56-63. DOI: 10.1016/j.isprsjprs.2012.08.003

Polunin O, Everard B. 1969. Flowers of Europe: A Field Guide. Oxford University Press: Oxford

Raupach M, Shaw R. 1982. Averaging procedures for flow within vegetation canopies. Boundary-Layer Meteorology **22**: 79-90. DOI: 10.1007/BF00128057

Riegl. 2015. Riegl Laser Measurement Systems; Riegl VZ-1000 datasheet. Riegl: www.riegl.com/.

Rusu RB, Marton ZC, Blodow N, Dolha M, Beetz M. 2008. Towards 3D Point cloud based object maps for household environments. Robotics and Autonomous Systems **56**: 927-941. DOI: 10.1016/j.robot.2008.08.005

Sand-Jensen K. 2003. Drag and reconfiguration of freshwater macrophytes. Freshwater Biology **48**: 271-283. DOI: 10.1046/j.1365-2427.2003.00998.x

Sand-Jensen K, Madsen T. 1992. Patch dynamics of the stream macrophyte, Callitriche cophocarpa. Freshwater Biology **27**: 277-282. DOI: 10.1111/j.1365-2427.1992.tb00539.x

Schoelynck J, Meire D, Bal K, Buis K, Troch P, Bouma T, Meire P, Temmerman S. 2013. Submerged macrophytes avoiding a negative feedback in reaction to hydrodynamic stress. Limnologica - Ecology and Management of Inland Waters **43**: 371-380. DOI: 10.1016/j.limno.2013.05.003

Schoneboom T, Aberle J, Dittrich A. 2010. Hydraulic resistance of vegetated flows: Contribution of bed shear stress and vegetative drag to total hydraulic resistance. In *River Flow*: Braunschweig, Germany; 269-276.

Simpson RL. 2001. Junction Flows. Annual Review of Fluid Mechanics **33**: 415-443. DOI: doi:10.1146/annurev.fluid.33.1.415

Siniscalchi F, Nikora VI. 2012. Flow-plant interactions in open-channel flows: A comparative analysis of five freshwater plant species. Water Resources Research **48**: W05503. DOI: 10.1029/2011WR011557

Stace CA. 2010. New flora of the British Isles. Cambridge University Press: Cambridge, UK

Stoesser T, Kim S, Diplas P. 2010. Turbulent Flow through Idealized Emergent Vegetation. Journal of Hydraulic Engineering **136**: 1003-1017. DOI: 10.1061/(ASCE)HY.1943-7900.0000153

Stoesser T, Salvador G, Rodi W, Diplas P. 2009. Large Eddy Simulation of Turbulent Flow Through Submerged Vegetation. Transport in Porous Media **78**: 347-365. DOI: 10.1007/s11242-009-9371-8

Straatsma MW, Warmink JJ, Middelkoop H. 2008. Two novel methods for field measurements of hydrodynamic density of floodplain vegetation using terrestrial laser scanning and digital parallel photography. International Journal of Remote Sensing **29**: 1595-1617. DOI: 10.1080/01431160701736455

Sukhodolov A, Sukhodolova T. 2010. Case Study: Effect of Submerged Aquatic Plants on Turbulence Structure in a Lowland River. Journal of Hydraulic Engineering **136**: 434-446. DOI: 10.1061/(ASCE)HY.1943-7900.0000195

Sukhodolov A, Sukhodolova T. 2014. Shallow wake behind exposed wood-induced bar in a gravel-bed river. Environmental Fluid Mechanics **14**: 1071-1083. DOI: 10.1007/s10652-013-9324-1

Tanino Y, Nepf H. 2008. Laboratory Investigation of Mean Drag in a Random Array of Rigid, Emergent Cylinders. Journal of Hydraulic Engineering **134**: 34-41. DOI: 10.1061/(ASCE)0733-9429(2008)134:1(34)

Tempest JA, Möller I, Spencer T. 2015. A review of plant-flow interactions on salt marshes: the importance of vegetation structure and plant mechanical characteristics. Wiley Interdisciplinary Reviews: Water **2**: 669–681. DOI: 10.1002/wat2.1103

807 Usherwood JR, Ennos AR, Ball DJ. 1997. Mechanical and anatomical adaptations in
808 terrestrial and aquatic buttercups to their respective environments. Journal of
809 Experimental Botany **48**: 1469-1475. DOI: 10.1093/jxb/48.7.1469

810
811 Valiela I, Teal JM, Deuser WG. 1978. The Nature of Growth Forms in the Salt Marsh
812 Grass Spartina alterniflora. The American Naturalist **112**: 461-470. DOI:
813 10.2307/2460116

814
815 Wilson C, Stoesser T, Bates P, Pinzen A. 2003. Open Channel Flow through
816 Different Forms of Submerged Flexible Vegetation. Journal of Hydraulic Engineering
817 **129**: 847-853. DOI: 10.1061/(ASCE)0733-9429(2003)129:11(847)

818
819 Wilson CAME, Stoesser T, Bates PD. 2005. Modelling of Open Channel Flow
820 through Vegetation. In *Computational Fluid Dynamics*. John Wiley & Sons, Ltd; 395-
821 428.

822
823 Wooding RA, Bradley EF, Marshall JK. 1973. Drag due to regular arrays of
824 roughness elements of varying geometry. Boundary-Layer Meteorology **5**: 285-308.
825 DOI: 10.1007/BF00155238

826
827 Yakhot V, Orszag S. 1986. Renormalization group analysis of turbulence. I. Basic
828 theory. Journal of Scientific Computing **1**: 3-51. DOI: 10.1007/BF01061452

829
830 Yue W, Parlange M, Meneveau C, Zhu W, Hout R, Katz J. 2007. Large-eddy
831 simulation of plant canopy flows using plant-scale representation. Boundary-Layer
832 Meteorology **124**: 183-203. DOI: 10.1007/s10546-007-9173-x

833

834